Molecularly Resolved Protein Electromechanical Properties

Daniel Axford,[†] Jason J. Davis,*[,†] Nan Wang,[†] Dongxu Wang,[‡] Tiantian Zhang,[‡] Jianwei Zhao,*[,‡] and Ben Peters[†]

Chemical Research Laboratory, Mansfield Road, University of Oxford, Oxford OX1 3TA, United Kingdom, Key Laboratory of Analytical Chemistry for Life Science (EMC), Department of Chemistry, Nanjing University, Nanjing 210093, People's Republic of China

Received: January 12, 2007; In Final Form: April 4, 2007

Previous work has shown that protein molecules can be trapped between the conductive surfaces presented by a metal-coated AFM probe and an underlying planar substrate where their molecule-specific conductance characteristics can be assayed. Herein, we demonstrate that transport across such a derived metal−protein−electrode junction falls within three, pressure-dependent, regimes and, further, that pressure-dependent conductance can be utilized in analyzing temporal variations of protein fold. Specifically, the electronic and mechanical properties of the metalloprotein azurin have been characterized under conditions of anisotropic vertical compression through the use of a conducting atomic force microscope (CP-AFM). By utilizing the ability of azurin to chemically self-assemble on the gold surface presented either by the apex of a suitably coated AFM probe or a planar metallic surface, molecular-level transport characteristics are assayable. Under conditions of low force, typically less than 2 nN, the weak physical and electronic coupling between the protein and the conducting contacts impedes tunneling and leads to charge buildup followed by dielectric breakdown. At slightly increased force, 3−5 nN, the copper protein exhibits temporal electron occupation with observable negative differential resistance, while the redox-inactive zinc mutant does not. At imposed loads greater than 5 nN, appreciable electron tunneling can be detected even at low bias for both the redox-active and -inactive species. Dynamic current−voltage characteristics have been recorded and are well-described by a modified Simmons tunneling model. Subsequent analyses enable the electron tunneling barrier height and barrier length to be determined under conditions of quantified vertical stress. The variance observed describes, in essence, the protein's mechanical properties within the confines of the tunnel junction.

1. Introduction

Understanding the molecule-level relationship between protein-mediated electron transfer and structure is of considerable significance not only in enhancing our understanding of events central to life,[1] but also in the potential exploitation of novel derived molecular devices.[2−5] To date, significant experimental effort has been applied to bioelectrochemical and bioelectronic analyses at both the macro- and nanoscales.[2,6−10] These studies have not only clarified the relationship between structure and tunnel conductance but also refined our ability to interface these molecules to man-made electrodes.

Experimental analyses of protein mechanical unfolding are numerous and increasingly highly refined.[11−13] The effects of compression have been, in contrast, subject to only minimal consideration[14] despite the fact that these equivalently play a potentially important role in the dynamic response of a protein fold to its environment.[15] Since structure and tunnel conductance are intrinsically linked, a time-resolved analysis of the latter can facilitate an understanding of molecular-level protein dynamics under conditions of quantified compressive force. The conducting atomic force microscope (CP-AFM) experimental configuration, in which tip deflection and electronic characterization are decoupled, enables a direct examination of the effects of molecular perturbation on tunnel transport.[16−18] A blue copper protein, azurin, which plays an important role in respiratory and photosynthetic electron transport chains[19] and is in possession of a redox-switchable copper center, has been chosen as the experimental sample in the work described herein, along with a redox-inactive mutant in which the copper is replaced by a zinc center. The molecule contains a surface disulfide group that may serve as an anchor in the formation of stable adlayers on Au(111) with the metal center oriented away from the surface.[20−22] In this study we have chemisorbed the protein at gold-coated AFM tips or a planar evaporated film and subsequently trapped it between electrode contacts on engaging the probe at gold or highly oriented pyrolytic graphite (HOPG) surfaces under force feedback.[23,24]

A combined theoretical analysis and simulation of transport characteristics enables protein deformation to be deduced directly from the compressive force dependence of conductance.[10,25] Generally, the electron transfer between two planar conducting electrodes that are separated by a thin layer of insulator and a voltage drop V can be described well by the Simmons model,[26] which gives current density as

$$i = \frac{e^2}{2\pi hL^2}\left\{\left(\varphi_0 - \frac{V}{2}\right)\exp\left[-K\left(\varphi_0 - \frac{V}{2}\right)^{1/2}\right] - \left(\varphi_0 + \frac{V}{2}\right)\exp\left[-K\left(\varphi_0 + \frac{V}{2}\right)^{1/2}\right]\right\} \quad (1)$$

where

* Corresponding authors. (J.Z.) Telephone/fax: +86-25-83596523. E-mail: zhaojw@nju.edu.cn. (J.J.D.) Telephone/fax: +44-1865 275914. E-mail: jason.davis@chem.ox.ac.uk.
[†] University of Oxford.
[‡] Nanjing University.

10.1021/jp070262o CCC: $37.00
Published on Web 07/12/2007

$$K = \frac{4\pi L}{h}(2me)^{1/2} \quad (2)$$

L is the barrier length, φ_0 is the mean barrier height, and e and m are the electron charge and mass, respectively. Due to the asymmetry of the tip−protein−substrate junction, a more appropriate treatment is to divide the voltage drop into two nonequivalent components as follows:

$$V = \alpha V + (1 - \alpha)V \quad (3)$$

where αV and $(1 - \alpha)V$ are the potential shifts at tip and substrate, respectively. The net current density is then modified to

$$i = \frac{e^2}{2\pi hL^2}\{(\varphi_0 - \alpha V)\exp[-K(\varphi_0 - \alpha V)^{1/2}] - [\varphi_0 + (1 - \alpha)V]\exp[-K(\varphi_0 + (1 - \alpha)V)^{1/2}]\} \quad (4)$$

Equation 4 gives a relationship between current and bias with three structure-related variables, namely φ_0, L, and an asymmetry factor, α. A detailed comparison of protein molecular conductance at various compressions thus facilitates considerable insight into deformation. Although the tunneling barrier height and length are correlated in the theoretical fitting, a deconvolution is possible.[27]

At low voltages, a more convenient form of eq 4 can be derived by linear approximation near $V \approx 0$ as

$$i = \left(\frac{e}{h}\right)^2\left[\frac{(2m)^{1/2}}{L}\right]\varphi_0{}^{1/2}V\exp(-K\varphi_0{}^{1/2}) \quad (5)$$

in which the $I-V$ relationship involves both barrier height and length.

2. Materials and Methods

2.1. Materials. Azurin (*Pseudomonas aeruginosa* azurin wild-type) was kindly supplied by Professor Gerard Canters, Leiden Institute of Chemistry, Leiden. It was diluted in ca. 0.1 M acetate buffer (pH 4.6, close to the protein isoelectric point) to form ca. 5 μM solution characterized by UV−vis spectroscopy (Lambda 20, Perkin-Elmer Ltd.) with $\epsilon_{279\,nm} = 9800\ M^{-1}\ cm^{-1}$.

2.2. Conducting AFM Measurements. *2.2.1. Tip−Protein Modification.* Gold-coated CP-AFM probes (Si_3N_4 contact probes, spring constant = 2.0 N/m, Mikromasch) were washed copiously with acetone, ethanol, and deionized water (Millipore, 18.2 MΩ·cm), and then modified with azurin by soaking in solution (~5 μM azurin, acetate buffer, pH 4.6) for at least 3 h. After incubation, the probes were rinsed copiously with deionized water to remove physically adsorbed material, blown dry with high-purity argon, and placed in the microscope. The tip was then brought into low force (<1 nN) contact with freshly cleaved HOPG. Molecular-level characterization was performed using CP-AFM (Pico SPM, Molecular Imaging) in contact mode where electrical characteristics were recorded independent of force feedback. $I-V$ curves were recorded for each force under scanned bias (given as tip bias with respect to the substrate). Nonlinear-least-squares fitting was performed with Origin 7.0 software and terminated at the point where a stable chi-squared value was achieved. All experiments were done under ambient conditions (22 ± 2 °C, 30−40% humidity).

2.2.2. Surface−Protein Modification. Gold-on-glass substrates (Arrandee) were annealed in a butane flame to create atomically flat terraces and allowed to cool before incubation in protein solution (5 μM protein, 40 mM HEPES buffer, pH 7.0) for at least 12 h at 4 °C. The surfaces were rinsed copiously with deionized water and dried under a nitrogen flow. The environmental chamber of the CP-AFM was flushed with nitrogen to reduce the presence of atmospheric water to a humidity of ~20−25%. The molecular surfaces were engaged with gold-coated AFM probes (spring constant 2.0 N/m, Mikromasch) at minimal force (<2.0 nN). The force was increased stepwise, and several hundred $I-V$ curves were taken at each force. The force regime studied was in the 2−5 nN range; additional $I-V$ data were taken at higher forces with the surface under dry toluene for comparison. Automated fitting of the Simmons equation to hundreds of $I-V$ curves was carried out utilizing the Origin 7.5 programming environment. A least squares fitting algorithm and automated data cycling was developed in-house.

3. Results and Discussion

3.1. Protein Matrix Conductance as a Function of Tip-Imposed Stress. *3.1.1. Dielectric Breakdown at Low Contact Force.* Under vertical forces of less than 2 nN, physical contact between the protein and electrodes is weak and, subsequently, the electron-transfer barrier is sufficiently wide and high so as to impede direct tip−substrate tunneling. Typical $I-V$ curves recorded during positive bias scan at a loaded force less than 2 nN via tip modification are shown in Figure 1a. A threshold voltage, before which no detectable current flows, of approximately 5.5 V can be deduced from these curves. Once the bias reaches this threshold the current jumps suddenly to the measurement limit (10 nA) of the preamplifier and is maintained at this magnitude as bias is reduced before inverting to −10 nA at zero bias. These observations were the same for both the Cu and Zn forms of the protein and independent of the junction preparation route (protein chemisorption at the tip or planar gold electrode; the former has been previously reported[28]). Similar behavior has been observed with alkyl self-assembled monolayers equivalently sandwiched between CP-AFM probes and planar substrates and has been attributed to dielectric breakdown.[29−32] A scan speed dependence (dV/dt) of the breakdown voltage is observed and can be related to previously proposed mechanisms associated with charge accumulation.[33] An extension of this concept to protein junctions is valid and a consideration of charge accumulation leads to a natural explanation of the observed scan rate dependency; a fast voltage ramp has an associated insufficient charge injection time and, accordingly, is associated with a shift in the breakdown voltage to higher fields. In the 0.5−10 V/s voltage ramp rate range, the breakdown voltage is constant at 3.0−4.2 V (0.6−1.4 GV/m), implying that injection/accumulation occurs effectively across this range.

3.1.2. Resonant Electron Tunneling under Moderate Force. The ability of electrons to access orbital states in an STM configuration may lead to highly potential-dependent imaging and, in some cases, negative differential resistance.[34−38,59] We propose here that, at low lever deflection (3−5 nN), the metal-coated AFM probe is only weakly electronically coupled to the protein and that the junction, in this way, resembles that in a typical scanning tunneling microscope (STM). Junction resistances at these forces are variable but broadly in the 100−800 GΩ range; this variance is indicative of weak probe−molecule electronic coupling. Figure 1b shows an $I-V$ trend of copper azurin obtained at a force of ~4 nN. The spectroscopic features, evident at both the positive and negative bias in 30−40% of analyses, are associated with 3−7-fold current increases above the linear regime and are consistent with resonant orbital access. They are observable with the protein chemisorbed at either the probe electrode or the planar electrode and are molecule-specific.

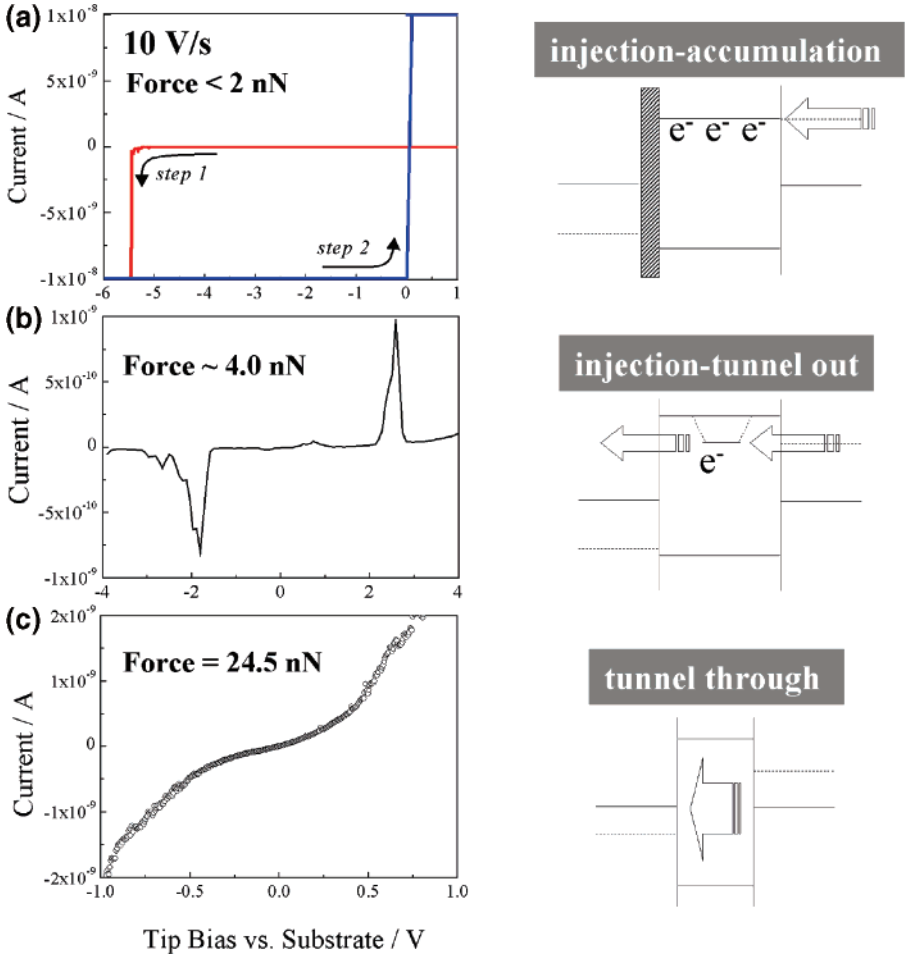

Figure 1. Representative current−voltage profiles, with associated schematics, of the three protein molecular conductance regimes. The force loads are (a) $F < 2$ nN, (b) $F \sim 4.0$ nN, and (c) $F = 24.5$ nN. All data shown here correspond to junction configurations in which the protein is chemisorbed on the planar electrode.

They are, notably, not observed with the nonredox-addressable zinc form of this protein (the zinc-based orbitals are of too low energy to be readily accessed) nor to any statistically relevant degree (<5%) in control experiments with other proteins[39] or saturated alkyl systems. A statistical analysis of current peak heights observed with the copper protein indicates considerable fluctuation in the voltage at which these current spikes are observed. Specifically, the peak center is observed at -2.2 ± 0.7 V for the negative bias and at 2.8 ± 1.0 V for the positive bias. We, and others,[35] have previously noted these peak fluctuations.

3.1.3. Electron-Transfer Characteristics under Force >5 nN. The chemisorbed protein adlayers, which are the subject of this report, are sufficiently robust for molecularly resolved near-field images to be acquired with comparative ease (Figure 2). In bringing gold AFM probes into mechanical contact with these surfaces, the spectroscopic features detailed in the previous section are resolvable at low force but disappear under conditions of increased probe-induced vertical stress. A typical $I-V$ curve obtained at 25 nN of contact force is shown in Figure 1c. Within a confined bias region (±50 mV), the current−voltage relationship is linear, with a low bias molecular resistance of $(1.4 \pm 0.3) \times 10^9\ \Omega$ being resolvable. This value lies close to those typically required for nondestructive STM imaging of these molecules.

The response becomes progressively nonlinear as bias excursions exceed ±50 mV. In Figure 1c, the current at +0.6 V (1.41×10^{-9} A) is 2-fold higher than that at −0.6 V (-6.82×10^{-10} A). This asymmetry cannot be adequately treated by the original Simmons formula (eq 1), but is well-described by the modified form (eq 4). Based on the (supported) conclusion that nonresonant (direct) electron tunneling is the dominant mechanism of charge transfer across these junctions under these conditions

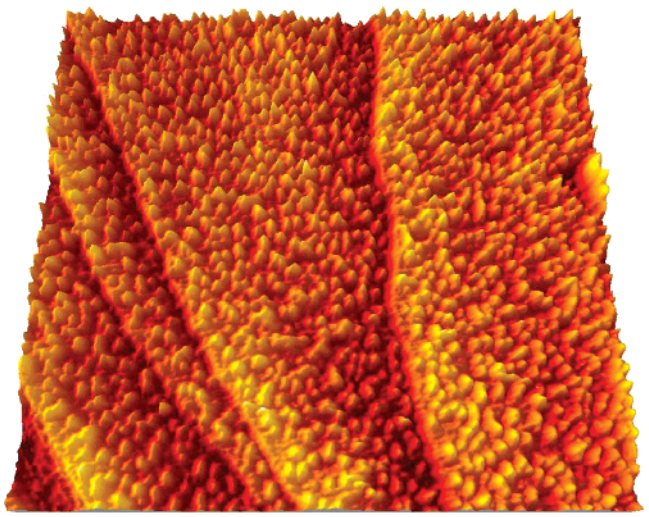

Figure 2. Electrochemical tunneling image of a typical surface assembled azurin monolayer on an evaporated film electrode. The image (340 × 340 nm), acquired under a water−glycerol mix (1:1) at room temperature at a tunneling current of 75 pA and tip bias = −0.700 V, demonstrates a good level of surface homogeneity and cleanliness. The coverage is estimated to be $(1-2) \times 10^{13}$ molecules/cm^2.

(the absence of any features in $I-V$ trends and indistinguishable Cu and Zn protein junction resistance), theoretical fitting with eq 4 resolves barrier heights and lengths of 1.0 eV and 0.95 nm respectively at 25 nN. The small barrier length suggests that appreciable molecular compression has taken place. The validity of this has been directly assessed through controlled force molecular imaging.[48]

To confirm that the tunneling characteristics being measured are not dominated by transport through water or other contaminants, the surface-modified substrate (Figure 2) was immersed in dry toluene for $I-V$ data analyses. The barrier height calculated at an applied load of 24 nN was 1.02 ± 0.06 eV with the associated decay parameter being 1.04 ± 0.06 Å^{-1}, in excellent agreement with that seen under ambient conditions at equivalent contact force (with the protein chemisorbed at either the probe electrode or the planar substrate electrode). We conclude that the presence of atmospheric water has little impact on the tunneling $I-V$ curves and that the tip- and surface-modification modalities provide equivalent information on electron transport through the protein.

3.1.4. Interpretation of Force Modulated Protein Electronics. In summarizing the three regimes of conductance described above (Figure 1), we can arrive at a fairly complete understanding of structure-related protein electron transfer. One can consider there to be three tunnel barriers active in these junctions, namely the barrier at the tip−protein interface, one associated with the polypeptide fold, and another at the protein−planar electrode interface. The magnitudes of these barriers, and so the ability of injected electrons to traverse them, are likely to be sensitive functions of molecule−electrode mechanical coupling. At low force, interfacial resistance arising from the weak physical contact at the probe interface plays an important role in the electron-transfer mechanism in that it exceeds the quantum unit of resistance R_Q ($h/e^2 \sim 26$ kΩ).[49] Though orbital states may be accessible at an appropriate bias, electron transport is impeded and charge consequently accumulates until dielectric breakdown results. On increasing the mechanical interaction between probe and protein (force load to 3−5 nN), the interfacial resistance becomes comparable to or less than R_Q, so tip−substrate electron tunneling becomes feasible. Further increases in probe−molecule contact lead to compression and a rapid narrowing of tunnel barrier and length. Under such conditions, direct electrode−electrode tunneling becomes facile. Simmons fitting to $I-V$ data indicates barrier lengths (effectively the height of the protein from the planar substrate electrode surface) of 1.5 ± 0.4 nm at 2.5 nN, 1.1 ± 0.04 nm at 5.1 nN, and 0.95 ± 0.03 at 25 nN. These values indicate that appreciable molecular compression takes place at all contact forces required to establish strong molecule−protein electronic coupling. As this coupling increases, conductance assays are subject to less scatter and the spectroscopic signatures associated with orbital occupancy disappear from the current−voltage plots of the redox-active copper protein. The perturbing impact of the analyzing probe electrode on the confined molecule precludes a reversible switching of junction transport between the "direct" and "ndr" regimes (analyses in the dielectric breakdown regime are likely to be associated with either removal of the molecule from the junction or its undefined destruction[29,30,32]). The nonelastic character of protein molecular compression has been previously reported.[50]

3.2. Dynamic Protein Deformation Characterized by Time-Resolved CP-AFM. On characterizing the conductance and transport characteristics of the protein across a range of probe contact forces, an attempt was made to analyze temporal variations in behavior. Specifically, in relating tunnel conductance to barrier length and height, temporal variance in electronic character can be interpreted through a consideration of force imparted protein conformational change. In the next section we discuss observations made in both small-incremental and large-sudden molecular compression regimes. These experiments were carried out with the protein chemisorbed to the probe electrode in order to minimize the effects of lateral piezo drift on molecular analyses.

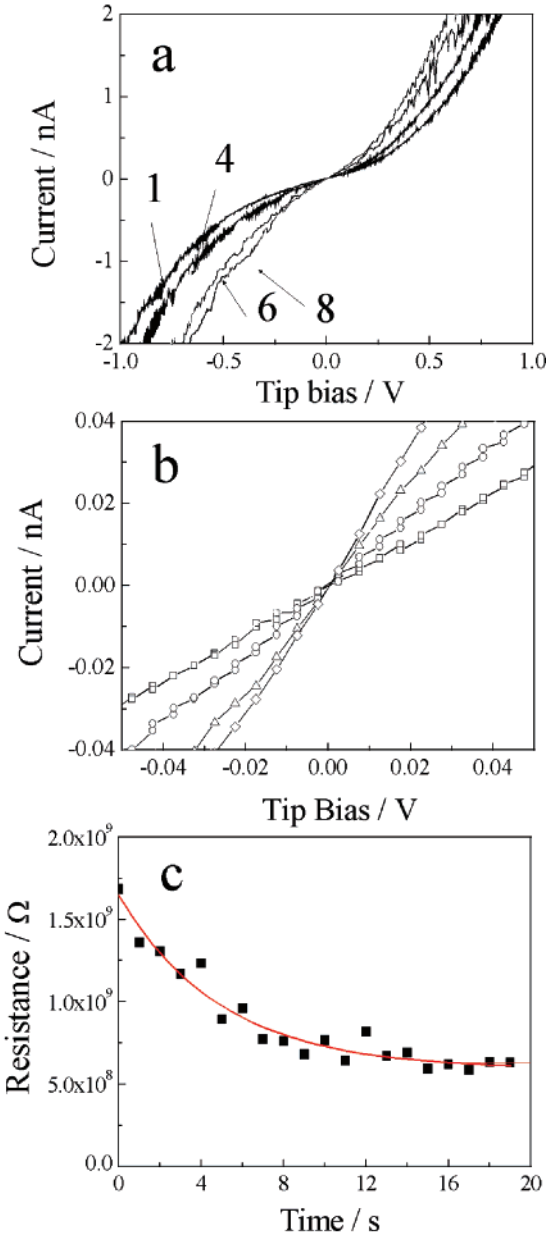

Figure 3. (a) Evolution of current−voltage profiles recorded at 1, 4, 6, and 8 s after a 6.3 nN force jump from a 12.6 nN starting point. (b) The corresponding small bias region from −50 to 50 mV. (c) The associated time-dependent resistance (R) is as derived from the low bias gradients in (b). A theoretical fitting to a first-order decay is represented by the solid line.

3.2.1. Short Time Frame Protein Conformational Relaxation. After the application of an initial, quantified, low force, the protein junctions were established as previously described and left for 2−5 min to facilitate a stabilization of the induced deformation before forces were further, and incrementally, increased. $I-V$ trends were subsequently recorded at specific forces. Figure 3a shows a typical response recorded on the

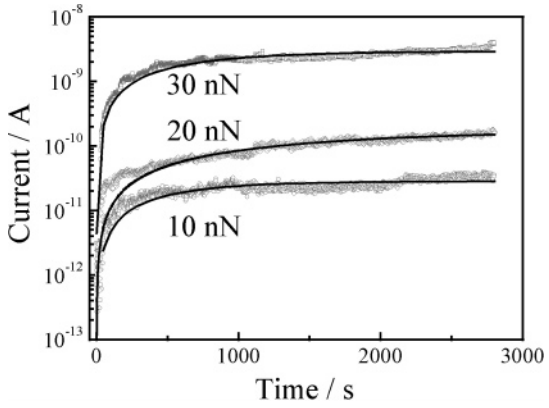

Figure 4. Long time frame evolution of current recorded at 0.1 V bias for different applied force jumps. Solid lines represent the theoretical fitting with a first-order decay.

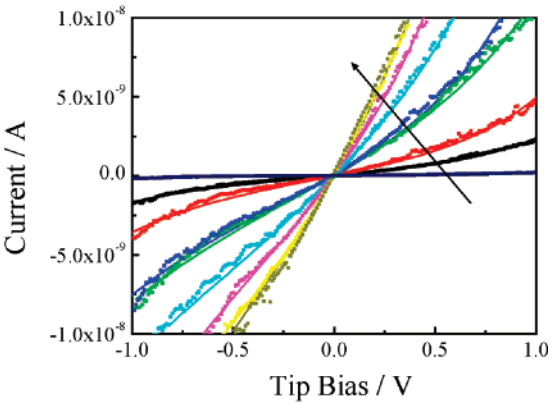

Figure 5. Evolution of $I-V$ curves under 20 nN compression, sequentially at 0, 1, 3, 6, 13, 20, 30, and 40 min. The solid lines give the theoretical predictions associated with the modified Simmons model (eq 4) in each case.

application of a 6 nN force increase (from 12 to 18 nN). In general, these trends were nonlinear as theoretically predicted for junctions of this type.[16,27] Incremental force increases of this magnitude were, predictably, accompanied by an associated decrease in tunnel resistance, an observation that can be ascribed to a decrease of either tunneling barrier height (φ_0) or tunneling distance (L), or a combination of both.

A Simmons formula fitting to the data shown in Figure 3a indicated only a minor modulation of these parameters with time once a force increment had been applied (comparative plots in Figure 3a and 3b). For example, in a 20-s time frame, φ_0 varied between 1.05 and 1.25 eV and L between 9.0 and 11.0 Å. An alternative treatment is to incorporate both φ_0 and L into an approximate formula for the small bias region near the voltage origin (eq 5, Figure 3b). The current is proportional to the bias with a slope (which has contributions from both φ_0 and L) which characterizes the protein resistance, R (eq 5). A typical time evolution of R is shown in Figure 3c, and is characterized by a rapid decrease on the immediate application of the perturbing force followed by a slower evolution, over approximately 10 s, to a relatively stable resistance plateau.

A further analysis of the protein deformation kinetics can be carried out by fitting temporal resistance change (Figure 3c) to an exponential decay equation:

$$R = R_\infty + (R_0 - R_\infty)\exp(-T/\tau_1) \qquad (6)$$

where R_∞ and R_0 are the resistances at infinite and zero time, respectively. τ_1 is the relaxation (decay) constant, indicating the

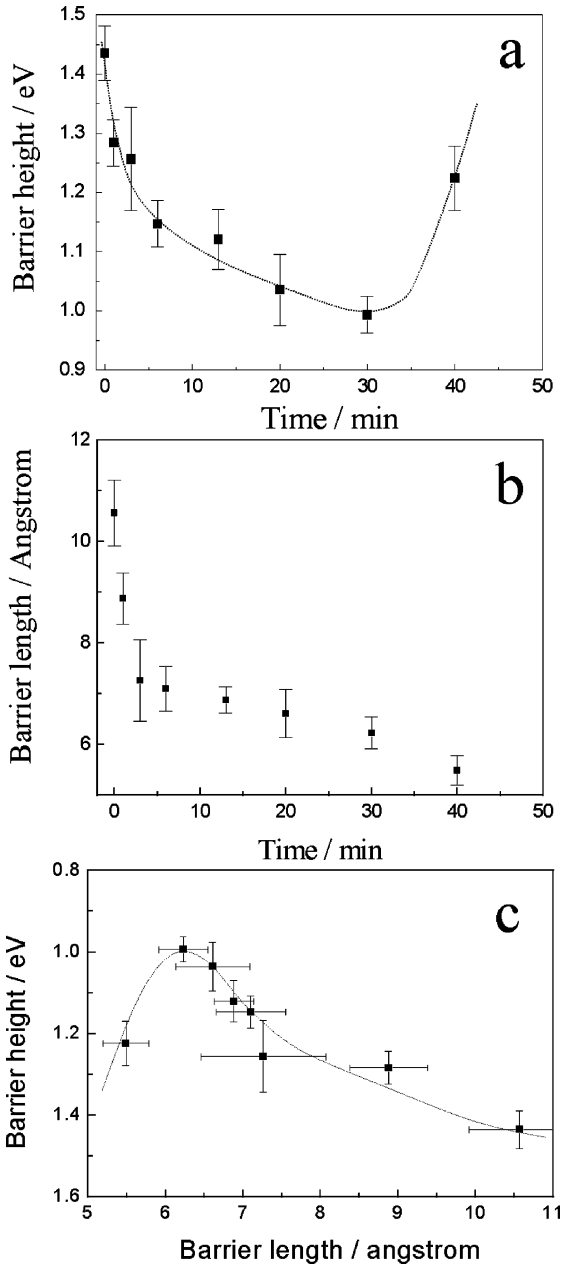

Figure 6. Time dependence of (a) barrier height (φ_0) and (b) barrier length (L) obtained by theoretical fitting of $I-V$ curves in Figure 4 by eq 4. (c) Correlation between barrier height (φ_0) and barrier length (L) summarized from (a) and (b).

time it takes the deviation $R-R_\infty$ to drop to $1/e$ of its initial value. Curve fittings resolve R_∞ and R_0 to be $(5.9 \pm 0.4) \times 10^8$ Ω and $(1.69 \pm 0.07) \times 10^9$ Ω, respectively. The key kinetic parameter, τ_1, defining the rate of molecular conductance change over time, is observed to be broadly constant, at 5.0 ± 0.7 s, in this force regime. These observations can be rationalized by considering the structural dynamics of the protein. The native protein is associated with a predominance of atoms held in relatively fixed positions in a conformational energy well. The native structure, with its secondary and tertiary elements, is maintained through stabilizing contributions from hydrogen bonds, salt bridges, van der Waals forces, and hydrophobic forces.[60] The rapid deformatory responses to applied force are consistent with an expectation of "free space" (atoms initially outside of van der Waals contact; see discussion below) in the protein fold. The establishment of a "plateau" of electrical conductance is likely to be related to the onset of repulsive

interactions in the protein as, for example, "like charges" are forced together. Though further anisotropic compression is possible, this requires greater force and, ultimately, is accompanied by significant geometric expansion of the protein fold in the lateral plane (see below).

3.2.2. Long Time Frame Protein Conformational Change under Constant Pressure. The response of the protein fold to sudden large (tens of nanonewtons) changes in anisotropic compression has also been examined.[61] Three current−time ($I-T$) curves, recorded at constant bias of 0.1 V, are shown in Figure 4. In all cases, there is an abrupt increase in conductance on initial application of the force jump, followed by a relatively stable plateau. These observations are consistent with rapid initial structural deformation (over a few tens of seconds) followed by a relatively slow (tens of minutes) extended deformation. Changes within the latter compressional regime are well-described by first-order exponential decay kinetics as

$$i = i_0[1 - \exp(-t/\tau_2)] \quad (7)$$

where τ_2 is the apparent relaxation (decay) constant for the extended protein deformation. i_0 denotes the saturated current at infinite time (both i_0 and τ_2 obtained by theoretical fitting to $I-T$ curves). The i_0 parameter, obtained by repeated fits to data, is found to increase by almost 1 order of magnitude for each 10 nN increase, an observation in good agreement with previous work.[23] The time constant, τ_2, varies between 500 and 1500 s, being almost 2 orders of magnitude longer than τ_1 (see previous section). These figures both support the suggestion that the slower evolution of protein fold has a different underlying mechanism and are consistent with related observations made by Zocchi et al.[14]

The force-induced changes in molecular resistance in this time regime are summarized by the trends shown in Figure 5 and can be reliably mapped by eq 4, from which associated barrier characteristics can be determined. By following the evolution of tunnel barrier height (Figure 6a), one observes an initial decrease over a few tens of minutes, followed by an increase. It is instructive at this point to note a direct correlation between φ_0 and the protein gross molecular structure. This parameter is related to the electron-transfer coefficient, β (in Å^{-1}), through eq 8:[26,52]

$$\beta = 1.025{\varphi_0}^{1/2} \quad (8)$$

Previous work has considered the effects of atomic packing on the ability of a protein matrix to mediate electronic flow and given an empirical expression to account for structure-dependent variations of the tunneling coefficient β:[1]

$$\beta = 0.9\rho + 2.8(1 - \rho) \quad (9)$$

In principle, the atom packing density ρ can range from 1, corresponding to a fully packed medium ($\beta \sim 0.9$ Å^{-1}), to a value of 0, corresponding to interstitial space in the protein structure ($\beta = 2.8$ Å^{-1}).[1,53] φ_0 is therefore correlated with the atomic packing density, through eq 8, by

$$\varphi_0 = (0.88\rho + 2.73(1 - \rho))^2 \quad (10)$$

It follows that, since packing density and barrier height are inversely related, force-induced compression will lead to an initial continuous decrease in barrier (and increase in conductance). When vertical forces are balanced by strong intramolecular repulsive interactions, one expects structural deformation to occur in the horizontal plane (where there is no spatial restriction). This is likely to be linked to a loss of major tertiary and secondary structure elements and a decrease of atomic packing density, i.e., increase in barrier height (Figure 6a). The tunneling barrier length is found to monotonically decrease as expected (Figure 6b). The relationship between barrier height and length is shown in Figure 6c, where φ_0 decreases before reaching a minimum and subsequently increases, as the protein is initially compressed. This trend is qualitatively comparable to expectations and molecular dynamics simulations (though the limitations of computing time necessarily constrain the time scales of the latter).[25]

It is worth drawing a comparison here between force-imposed protein compression and unfolding, the latter having been studied intensively.[11,54−57] In unfolding experiments, the applied force is (normally) required only to disrupt noncovalent interactions between the polypeptide chain and its associated side groups and typically lies in the range of a few hundred piconewtons. The force scales associated with the study reported herein are associated with progressions along the compressional regime of a Lennard-Jones potential profile, a considerably more energetically demanding process. The evolution of deconvoluted[58] tunnel length with either time or compressional force (Figure 6) gives insight into the mechanical properties of the molecular structure and, specifically, its response to perturbation. With increased molecular compression, atomic packing density increases and the associated barrier to tunneling across the structure falls. Under such conditions, the structure is likely to be more conformationally rigid and further application of pressure may lead to gross structural change, a proposition consistent with the increasing tunnel barrier in this regime (Figure 6a).

4. Concluding Remarks

In this work we have characterized the conductance characteristics of a redox switchable metalloprotein at a molecular level and resolved three, mechanically modulated, regimes of tunnel transport. The conductance characteristics of the protein as assayed through either tip or surface modification are equivalent. The copper and zinc forms of azurin display transport characteristics which are distinguishable only within the narrow force confines where resonant tunneling appears to be detected (the copper center plays a demonstrably important role in the appearance of negative differential resistance). Under conditions of more robust electrode−molecule electronic coupling, direct nonresonant tunneling dominates. In this regime the application of a Simmons tunneling model leads to an accurate description of transport characteristics and is further validated by the observation of equivalent conductance characteristics in a solvent medium under equivalent probe contact. The dynamic changes in protein fold under a variety of incremental changes in AFM probe/electrode applied compressional force have, additionally, been examined. The results highlight the dependence of protein structure and associated conductance characteristics on both proximal probe imparted stress amplitudes and time scales. We suggest that the time evolution of molecular conductance observed when these molecules are examined in such tunnel junctions reflects the combined effects of probe-induced perturbation and underlying protein structural mechanics.

Acknowledgment. This project was partially supported by the National Natural Science Foundation of China (Nos. 20435010, 20503012, 20521503). J.J.D. acknowledges financial support from the EPSRC (GR/S71811/01).

References and Notes

(1) Page, C. C.; Moser, C. C.; Chen, X.; Dutton, P. L. *Nature* **1999**, *402*, 47.
(2) Gilardi, G.; Fantuzzi, A.; Sadeghi, S. J. *Curr. Opin. Struct. Biol.* **2001**, *11*, 491.
(3) Katz, E.; Willner, I. *Angew. Chem., Int. Ed.* **2004**, *43*, 6042.
(4) Katz, E.; Willner, I.; Wang, J. *Electroanalysis* **2004**, *16*, 19.
(5) Maruccio, G.; Visconti, P.; Biasco, A.; Bramanti, A.; Torre, A. D.; Pompa, P. P.; Frascerra, V.; Arima, V.; DAmone, E.; Cingolani, R.; Rinaldi, R. *Electroanalysis* **2004**, *16*, 1863.
(6) Zhang, J.; Chi, Q.; Kuznetsov, A. M.; Hansen, A. G.; Wackerbarth, H.; Christensen, H. E. M.; Andersen, J. E. T.; Ulstrup, J. *J. Phys. Chem. B* **2002**, *106*, 1131.
(7) Forzani, E. S.; Zhang, H.; Nagahara, L. A.; Amlani, I.; Tsui, R.; Tao, N. *Nano Lett.* **2004**, *4*, 1785.
(8) Kharitonov, A. B.; Zayats, M.; Alfonta, L.; Katz, E.; Willner, I. *Sens. Actuators, B* **2001**, *76*, 203.
(9) Porath, D.; Bezryadin, A.; Vries, S. d.; Dekker, C. *Nature* **2000**, *403*, 635.
(10) Davis, J. J.; Morgan, D. A.; Wrathmell, C. L.; Axford, D. N.; Zhao, J.; Wang, N. *J. Mater. Chem.* **2005**, *15*, 2160.
(11) Sarkar, A.; Robertson, R. B.; Fernandez, J. M. *Proc. Natl. Acad. Sci. U.S.A.* **2004**, *101*, 12882.
(12) Fernandez, J. M.; Li, H. B. *Science* **2004**, *303*, 1674.
(13) Zhuang, X. W.; Bartley, L. E.; Babcock, H. P.; Russell, R.; Ha, J. J.; Herschlag, D.; Chu, S. *Science* **2000**, *288*, 2048.
(14) Singh-Zocchi, M.; Hanne, J.; Zocchi, G. *Biophys. J.* **2002**, *83*, 2211.
(15) Navizet, I.; Cailliez, F.; Lavery, R. *Biophys. J.* **2004**, *87*, 1426.
(16) Zhao, J.; Uosaki, K. *Nano Lett.* **2002**, *2*, 137.
(17) Wold, D. J.; Frisbie, C. D. *J. Am. Chem. Soc.* **2000**, *122*, 2970.
(18) Cui, Z. X.; Zarate, X.; Tomfohr, J.; Sankey, O. F.; Primak, A.; Moore, A. L.; Moore, T. A.; Gust, D.; Harris, G.; Lindsay, S. M. *Nanotechnology* **2002**, *13*, 5.
(19) Adman, E. T. *Adv. Protein Chem.* **1991**, *42*, 145.
(20) Davis, J. J.; Halliwell, C. M.; Hill, H. A. O.; Canters, G. W.; van Amsterdam, M. C.; Verbeet, M. P. *New. J. Chem.* **1998**, *22*, 1119.
(21) Chi, Q.; Zhang, J.; Andersen, J. E. T.; Ulstrup, J. *J. Phys. Chem. B* **2001**, *105*, 4669.
(22) Davis, J. J.; Bruce, D.; Canters, G. W.; Crozier, J.; Hill, H. A. O. *Chem. Commun.* **2003**, 576.
(23) Zhao, J. W.; Davis, J. J. *Nanotechnology* **2003**, *14*, 1023.
(24) Alessandrini, A.; Salerno, M.; Frabboni, S.; Facci, P. *Appl. Phys. Lett.* **2005**, *86*, 133902.
(25) Zhao, J.; Davis, J.; Sansom, M.; Hung, A. *J. Am. Chem. Soc.* **2004**, *126*, 5601.
(26) Simmons, J. G. *J. Appl. Phys.* **1963**, *34*, 1793.
(27) Zhao, J.; Davis, J. J. *Colloids Surf., B: Biointerfaces* **2005**, *40*, 189.
(28) Davis, J. J.; Wang, N.; Morgan, D.; Zhang, T.; Zhao, J. *Faraday Discuss. Chem Soc.* **2006**, *131*, 167.
(29) Wold, D.; Frisbie, C. *J. Am. Chem. Soc.* **2001**, *123*, 5549.
(30) Boulas, C.; Davidovits, J. V.; Rondelez, F.; Vuillaume, D. *Phys. Rev. Lett.* **1996**, *76*, 4797.
(31) Ara, M.; Graaf, H.; Tada, H. *Appl. Phys. Lett. 18*, 2565.
(32) Zhao, J. W. U., K. *Appl. Phys. Lett.* **2003**, *83*, 2034.
(33) Luo, E. Z.; Lin, S.; Xie, Z.; Xu, J. B.; Wilson, I. H.; Yu, Y. H.; Yu, L. J.; Wang, X. *Mater. Charact.* **2002**, *48*, 205.
(34) Xue, Y. *Phys. Rev. B 59*, R7852.
(35) Gorman, C.; Carroll, R.; Fuierer, R. *Langmuir* **2001**, *17*, 6923.
(36) He, J.; Lindsay, S. M. *J. Am. Chem. Soc.* **2005**, *127*, 11932.
(37) He, J.; Fu, Q.; Lindsay, S.; Ciszek, J. W.; Tour, J. M. *J. Am. Chem. Soc.* **1996**, *128*, 14828.
(38) Xiao, X.; Nagahara, L. A.; Rawlett, A. M.; Tao, N. *J. Am. Chem. Soc.* **2005**, *127*, 9235.
(39) Axford, D. N.; Davis, J. J. *Nanotechnology* **2007**, *18*, 145502.
(40) Shi, X.; Zheng, X.; Dai, Z.; Wang, Y.; Zeng, Z. *J. Phys. Chem B* **2005**, *109*, 3334.
(41) Chen, J.; Wang, W.; Reed, M. A.; Rawlett, A. M.; Price, D. W.; Tour, J. M. *Appl. Phys. Lett.* **2000**, *77*, 1224.
(42) Tivanski, A. V.; Walker, G. C. *J. Am. Chem. Soc.* **2005**, *127*, 7647.
(43) Wassel, R. A.; Credo, G. M.; Fuierer, R. R.; Feldheim, D. L.; Gorman, C. B. *J. Am. Chem. Soc.* **2004**, *126*, 295.
(44) Guisinger, N. P.; Greene, M. E.; Basu, R.; Baluch, A. S.; Hersam, M. C. *Nano Lett.* **2004**, *4*, 55.
(45) Cornil, J.; Karzazi, Y.; Bredas, J. L. *J. Am. Chem. Soc.* **2002**, *124*, 3516.
(46) Fan, F. R. F.; Yang, J.; Cai, L.; Price, D. W.; Dirk, S. M.; Kosynkin, D. V.; Yao, Y.; Rawlett, A. M.; Tour, J. M.; Bard, A. J. *J. Am. Chem. Soc.* **2002**, *124*, 5550.
(47) Datta, S. Cambridge University Press: 1995.
(48) Davis, J. J.; Wang, N.; Morgan, D.; Zhang, T.; Zhao, J. *Faraday Discuss. Chem Soc.* **2006**, *131*, 167.
(49) Zhao, J.; Uosaki, K. *J. Phys. Chem B* **2004**, *108*, 17129.
(50) Zhao, J.; Davis, J. J.; Sansom, M. S. P.; Hung, A. *J. Am. Chem. Soc.* **2004**, *126*, 5601.
(51) Andolfi, L.; Bruce, D.; Cannistraro, S.; Canters, G. W.; Davis, J. J.; Hill, H. A. O.; Crozier, J.; Verbeet, M. P.; Wrathmell, C. L.; Astier, Y. *J. Electroanal. Chem.* **2004**, *565*, 21.
(52) Tian, W. D.; Datta, S.; Hong, S. H.; Reifenberger, R.; Henderson, J. I.; Kubiak, C. P. *J. Chem. Phys.* **1998**, *109*, 2874.
(53) Skourtis, S. S.; Beratan, D. N. *J. Biol. Inorg. Chem.* **1997**, *2*, 378.
(54) Moser, C. C.; Keske, J. M.; Warncke, K.; Farid, R. S.; Dutton, P. L. *Nature* **1992**, *355*, 796.
(55) Bao, G. *J. Mech. Phys. Solids* **2002**, *50*, 2237.
(56) Kellermayer, M. S. Z.; Smith, S. B.; Granzier, H. L.; Bustamante, C. *Science* **1997**, *276*, 1112.
(57) Tskhovrebova, L.; Trinick, J.; Sleep, J. A.; Simmons, R. M. *Nature* **1997**, *387*, 308.

(58) These values span a sufficiently large range over the force/time spans used here that deconvolution of barrier height and length is effective.

(59) Several mechanisms of negative differential resistance have been proposed. We consider here the effects of redox-related charge accumulation and note that there is no absolute requirement for the probe to have a noncontinuous density of states.[36,40−47]

(60) Though it is not possible to directly probe the retention or otherwise of protein fold in molecules chemisorbed and confined to a tunnel junction, previous topographic and electroanalytical investigations of these adlayers have given molecular dimensions and half-wave redox potentials consistent with the native structure (prior to the probe perturbation inherent in experiments of this type).[22,48,51]

(61) Any potential loss of protein from the confines of the tunnel junction is signaled by a dramatic change in current−voltage characteristics as direct electrode−electrode contact is established.